



HAL
open science

Estimation the reactive surface area of minerals during fluid-rock interaction in hydrothermal Jiangxi Province (SE China)

E. Zippa, P. Zuddas

► **To cite this version:**

E. Zippa, P. Zuddas. Estimation the reactive surface area of minerals during fluid-rock interaction in hydrothermal Jiangxi Province (SE China). *Applied Geochemistry*, 2020, 120, pp.104675 -. 10.1016/j.apgeochem.2020.104675 . hal-03491210

HAL Id: hal-03491210

<https://hal.science/hal-03491210>

Submitted on 22 Aug 2022

HAL is a multi-disciplinary open access archive for the deposit and dissemination of scientific research documents, whether they are published or not. The documents may come from teaching and research institutions in France or abroad, or from public or private research centers.

L'archive ouverte pluridisciplinaire **HAL**, est destinée au dépôt et à la diffusion de documents scientifiques de niveau recherche, publiés ou non, émanant des établissements d'enseignement et de recherche français ou étrangers, des laboratoires publics ou privés.



Distributed under a Creative Commons Attribution - NonCommercial 4.0 International License

ESTIMATION THE REACTIVE SURFACE AREA OF MINERALS DURING FLUID-ROCK INTERACTION IN HYDROTHERMAL JIANGXI PROVINCE (SE CHINA)

E. Zippa^{a,b}, P. Zuddas^a

^a*Sorbonne University, METIS, , 4 Jussieu, F75005 Paris, France*

^b*Tomsk Branch of the Trofimuk Institute of Petroleum Geology and Geophysics in the Siberian Branch of the Russian Academy of Sciences, 634021, Tomsk, Akademicheskii 4, Russia*

Abstract

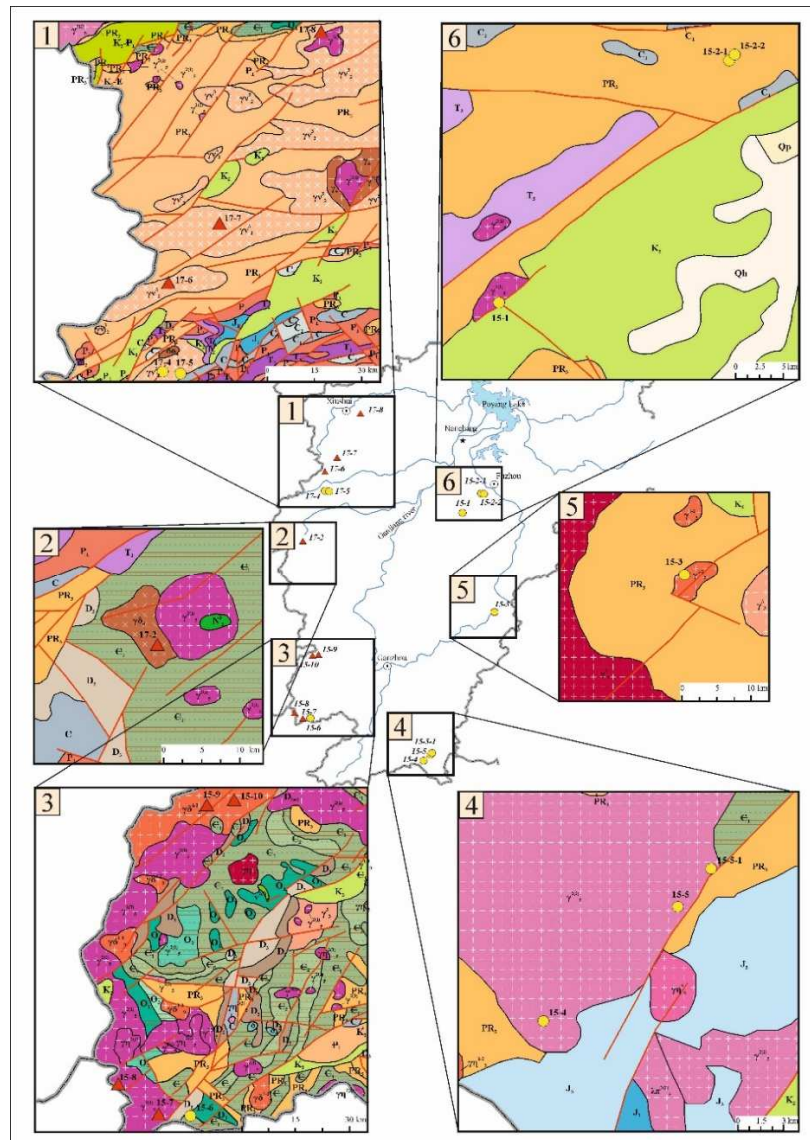
The reactive surface areas of the most abundant reacting minerals have been estimated in the granite hydrothermal field of Jiangxi Province in South-East China. The chemical composition of the sampled fluids was used as input data and the continuous equilibrium approach was assumed for the kinetic calculations. Dissolution rates and the reactive surface areas of different minerals were obtained by reconstructing the chemical evolution of the interacting fluids in a reaction process schema defined by a fractional degree of advance of the irreversible mass-transfer process. We found that the reactive surface area ratio of albite/K-feldspar varies by 2-3 orders of magnitude while that of biotite/ K-feldspar ratio by 4 orders of magnitude. The obtained results indicate that mineral reactive surface areas are not constant during the fluid-granite interaction: higher reactive surface areas were obtained at higher pCO₂ partial pressure (lower pH) compared to water with lower pCO₂ partial pressure (higher pH). The eventual formation of secondary clay-minerals overlaying the primary ones may be responsible for decreasing the contact area of the rock-forming mineral in thermal waters having higher pH. The results of our investigation indicate that the reactive surface area of biotite play an important role in the CO₂-neutralizing process of this area that in turn, controls the natural releasing of CO₂ to the atmosphere in this area.

Keywords: reactive surface area, water-rock interaction, CO₂ influence on the water-rock interaction, thermal waters

1. Introduction

The hydrothermal Jiangxi Province, located in southeastern China is characterized by approximately 96 hot springs within a distance from 5 to 50 Km (Li, 1979; Zhou, 1996; Sun and Li, 2001) with different composition and CO₂ partial pressure at the emergence (Li, 1979; Zhou, 1996; Sun and Li, 2001; Sun et al., 2016; Shvartsev et al., 2018). These thermal springs occur along deep faults extending for several hundred kilometers along strike where earthquakes of various intensity have been observed (Zhou, 1996). This region is characterized by two regional

36 tectonic units: the Yangtze platform in the North Jiangxi and the South China Fold System in the
37 Central-Southern Jiangxi. The thermal waters predominantly occurs within granitoids (Figs 1
38 and 2) consisting of K-feldspar, (mainly microcline 30-35%), plagioclase (mainly albite, 25-
39 30%), quartz (30-35%) and biotite (8-10%) (Wang et al., 2012; Tao et al., 2018). Previous
40 investigations on the thermal waters in Jiangxi Province (Sun et al., 2016; Zipa, 2017; Sun et
41 al., 2017; Shvartsev et al., 2018) investigated geochemical peculiarities such as saturation state
42 with respect to different minerals explaining possible mechanisms controlling the different
43 composition of the springs. Previously, Chen (2008) and Sun et al. (2014) recorded the
44 $\delta^{13}\text{C}(\text{CO}_2)$ varying from -5,50 to -3,49 ‰ and indicated that CO_2 is from mantle or magmatic
45 origin in this degassing area. In this work, we want to test the effect of CO_2 raising from deep
46 that potentially influence the water chemical composition by dissolution and precipitation
47 reactions. We attempt to evaluate the mineral reactivity in response to the raising CO_2 and offer
48 an estimation of reactive surface areas (RSA) of the main rock-forming minerals. RSA of
49 minerals is an important parameter in modelling geochemical kinetic studies since affects the
50 magnitude of mineral dissolution modulating the CO_2 rising to the atmosphere (Bolourinejad et
51 al., 2014). RSA of minerals has been generally estimated under experimental laboratory
52 conditions and is often assumed to be invariable in geochemical modelling of mineral reactivity
53 at the field scale even if this strong approximation makes unrealistic many reactive transport
54 modelling results (Gouze and Luquot, 2011). Here, we attempt to estimate the RSA of the main
55 rock-forming minerals using the water chemical composition as input data as they reflect the
56 realistic reactivity at the natural field scale.



57

58

Fig.1. Geological map of Jiangxi Province

Quaternary period	Qh	Holocene. Alluvial deposits: sand, gravel, clay.
	Qp	Pleistocene. Alluvial deposits: gravel, clay, coarse sand, moraine.
	N	Neogene. Sand, siltstone, peat.
	P ₁	Paleocene. Brick-red conglomerates, sand, siltstone, sandstone.
Jurassic period	K ₂ -P ₁	Paleocene and Upper-Cretaceous. Undivided.
	K ₂	Upper-Cretaceous. Dark-purple sandstone, brick-red conglomerates, sandstone, siltstones, mudstone.
	J ₃	Upper. Sand shale, conglomerate, volcanic tuff, andesite.
Triassic period	J ₁	Lower. Feldspar, quartz sandstone, sand, gravel, sand shale, even a thin coal seam
	T ₃	Upper. Conglomerates, sand shale, mudstone, coal shales and coal seams.
Permian period	T ₁	Lower. Brown-red mudstone, siltstone and limestone slate.
	P ₂	Upper. Limestone, siliceous limestone, sand shale, mudstone and interlayers of coal.
Carboniferous period	P ₁	Lower. Limestone, coal seams, siliceous rocks, carbonaceous mudstones and coal shales.
	C ₂	Upper. Limestone, dolomite limestone, dolomite.
Devonian period	C ₁	Lower. Conglomerate, sand shale, mudstones.
	D ₃	Upper. Sand shale, siltstone, mudstone, disseminated hematite.
Ordovician period	D ₂	Lower. Conglomerates, siltstone, mudstone, inclusions of dolomite limestone.
	O ₃	Upper. Limestone, limestone mudstone (north of Jiangxi), sand shale and coal-siliceous shale (south of central Jiangxi).
	O ₂	Middle. Limestone, mudstones and clayey mudstones (north of Jiangxi), coal-bearing shale and sandstone (south of central Jiangxi).
Cambrian period	O ₁	Lower. Limestone, lenticular limestone and limestone mudstone (north of Jiangxi), sand shale, carbonaceous and siliceous shale (south of Jiangxi)
	Є ₂	Middle. Limestone, dolomite limestone (north of Jiangxi), interspersed carbon shale in the sand (south of the central part of Jiangxi).
Proterozoic era	Є ₁	Lower. Carbon-containing siliceous shale, siltstone, dolomite and coal seams (north of Jiangxi), sand shale, tufogenic sandstone and carbon-containing siliceous
	PR ₃	Upper. Limestone, silica, coal shale, siltstone, conglomerates, sandstone, tillite, tuff, phyllite and siliceous slate, sand slate, iron ore (magnetite) interlayers.
	PR ₂	Middle. Shale, phyllite, metamorphic sandstone, mafic (Fe, Mg) lava.

LEGEND

MAGMATIC ROCKS

Upper-Jurassic - Lower-Cretaceous (J₃-K₁)

-  Rhyolite porphyry.
-  Granite.
-  Monzonite granite.

Lower-Jurassic - Middle-Jurassic (J₁-J₂)

-  Granite.
-  Monzonite granite.
-  Gabbro.

Permian-Triassic (P-T)

-  Granite.
-  Monzonite granite.

Devonian-Carboniferous (D-C)

-  Granite.
-  Granodiorite.
-  Quartz diorite.
-  Diorite.

Silurian (S)

-  Granite.
-  Monzonite granite.

Cambrian-Ordovician (Є-O)

-  Granite.
-  Granodiorite.

Upper-Proterozoic (PR)

-  Myarolite.
-  Undivided basic rocks.
-  Peridotite.

-  The first group of thermal waters
-  The second group of thermal waters
-  Province borders
-  Lake
-  River
-  Capital of the Province
-  City
-  Faults



Fig.2. The legend for Geological map of Jiangxi Province

61 **1. Methods**

62 The 18 springs were sampled between 2015 and 2017. In the field, we measured water
63 temperature, conductivity using an AMTAST AMT03 (USA) device previously calibrated and
64 pH was using a portable Thermo-Scientific Orior Star meter equipped with conventional glass
65 electrodes. Electrode calibration was carried out against 3 NIST buffers at the temperatures of
66 the springs. Samples were filtrated in the field using membrane filters with 0.45 μm pore size.
67 Alkalinity was determined in the field (and later in laboratory also) by titration using the Gran
68 method. Major elements were analysed in the laboratory: Ca^{2+} and Mg^{2+} were determined by
69 titration with a liquid analyser “Anion 7-51” (Russia); Cl^- , F^- , SO_4^{2-} , Na^+ , and K^+ were
70 determined by ion chromatography with a Dionex chromatograph ICS-1000 (USA). Silica and
71 aluminium were measured by Inductively Coupled Plasma NexION 300D device (PerkinElmer,
72 USA) with standard deviations less than 3%. Thermodynamic calculations, ions activity, solution
73 saturation state, and pCO_2 partial pressure were performed using the Geochemist's Workbench
74 (Bethke et al., 2018) and PhreeqC (the LLNL database, version 3.06 Parkhurst and and Appelo
75 2010) softwares .

76 **2. Results**

77 *2.1. The chemical composition of the thermal waters in Jiangxi Province*

78 The results of the analytical determination are reported in Table 1. The thermal waters
79 were classified into two groups in accordance with the calculated P_{CO_2} . First group includes
80 thermal waters with pCO_2 varying between 0.74×10^{-3} and 1460.28×10^{-3} atm. These springs
81 correspond to areas of CO_2 degassing. The second group includes springs with P_{CO_2} ranging
82 between 0.03 and 0.3×10^{-3} atm. that is close to the present average atmospheric level (10^{-4} atm).
83 Fig. 3 shows that the first group refers to waters with $\text{pH} < 8$ while the second corresponds to
84 water having $\text{pH} > 8$.

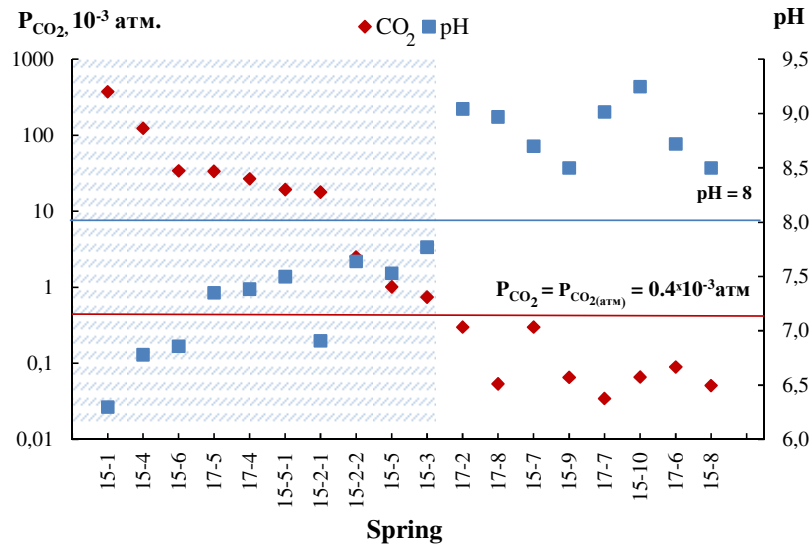


Fig. 3. The classification of thermal waters in Jiangxi Province

The first-group of thermal waters is characterized by the high TDS, pH ranging from 6.30 to 7.77 and salinity varying from 0.3 to 3.9 g/L (mean of 1.4 g/L). The predominant anion is bicarbonate ranging between 1.6 and 36.9 mmol/L, while sulfate is significantly lower (from 0.06 to 7.97 mmol/L) and chlorine does not exceed 2.3 mmol/L. Sodium dominates among cations with concentration varying from 0.07 to 42.17 mmol/L. Ca^{2+} and Mg^{2+} are lower ranging from 0.25 to 3.46 mmol/L, from 0.0021 to 0.65 mmol/L respectively, similarly to K^{+} that spans from 0.01 to 2.62 mmol/L. Silica and Al concentrations vary respectively from 0.26 to 1.96 mmol/L and from 0.1 to 1.3 $\mu\text{mol/L}$. This group of thermal waters belong to the $\text{HCO}_3\text{-Na}$ type.

The second-group has lower mineralization (0.26 to 0.42 g/L), higher pH (from 8.50 to 9.25) and $\text{HCO}_3\text{-Na}$ and $\text{HCO}_3\text{-SO}_4\text{-Na}$ chemical compositions (Tab. 1). In general, the bicarbonate ion is predominant among the anions ranging from 0.87 to 3.05 mmol/L while sulfate does not exceed 1.5 mmol/L. Sodium is the dominant cation ranging from 2.4 to 4.8 mmol/L. This second-group of waters is depleted in Ca^{2+} , K^{+} , and Mg^{2+} with concentrations lower than 0.5 mmol/L and enriched in F and Si with concentrations varying from 0.1 to 0.8 mmol/L and from 0.5 to 2.2 mmol/L respectively. The aluminum content ranges from 0.4 to 1.2 $\mu\text{mol/L}$.

Table 1. The chemical composition of the thermal waters in Jiangxi Province, mmol/L (Al is in $\mu\text{mol/L}$)

Spring	T, °C	pH	Alkalinity	SO_4^{2-}	Cl^-	Na^+	Ca^{2+}	Mg^{2+}	K^+	F^-	Si	Al_{tot}
<i>The first group</i>												
15-5-1	71	7.50	2.39	0.2396	0.1803	3.04	0.3100	0.0021	0.0692	0.6158	1.2788	0.4044
15-5	72	7.53	2.39	0.2708	0.2000	3.09	0.3050	0.0029	0.0949	0.7526	1.3784	0.4368
15-6	43	6.86	4.10	0.2604	0.1408	3.96	0.6125	0.0208	0.2128	0.4947	1.7770	1.2779
15-4	55	6.78	29.84	2.6771	1.0000	30.57	2.2500	0.2542	1.5179	0.3789	2.5077	1.0287
15-2-1	41	6.91	2.08	0.3958	0.0761	0.39	1.2750	0.1250	0.1538	0.2474	0.7473	0.1242
17-4	29	7.39	3.75	0.2781	0.0549	0.16	1.6225	0.4542	0.0200	0.0274	0.3006	0.3046

17-5	32	7.35	5.24	0.0635	0.0946	0.07	2.2250	0.5458	0.0144	0.0042	0.2674	0.3025
15-1	36	6.30	12.20	0.4479	0.3042	5.74	3.2500	0.6458	2.6205	0.2579	1.3286	1.0391
15-2-2	53	7.64	2.30	0.5208	0.0592	0.52	1.5450	0.1204	0.3897	0.2421	0.9466	0.0981
15-3	58	7.77	1.61	4.8438	0.4761	9.61	0.9750	0.0063	0.5000	0.5053	1.9597	0.5759
<i>The second group</i>												
17-2	27	9.05	2.05	0.1990	0.1296	2.71	0.1580	0.0017	0.0226	0.3211	0.5813	1.1247
17-8	59	8.97	1.92	0.2375	0.1372	3.19	0.1500	0.0002	0.0708	0.5684	0.5248	0.6146
15-7	38	8.70	2.29	0.1771	0.1746	3.13	0.0950	0.0008	0.0508	0.8211	1.1293	0.6308
15-9	82	8.50	2.26	0.1875	0.1211	3.30	0.1050	0.0021	0.1305	0.7684	1.9265	0.9678
17-7	55	9.02	1.11	0.5740	0.0431	2.41	0.1275	0.0021	0.0687	0.1474	1.4199	1.0173
15-10	41	9.25	1.61	0.5833	0.1690	3.91	0.0598	0.0013	0.0785	0.7684	1.8268	0.3794
17-6	54	8.72	1.33	1.0865	0.1887	3.59	0.2025	0.0020	0.0703	0.3000	1.3004	0.4242
15-8	83	8.50	1.85	0.4583	0.1099	2.57	0.1600	0.0058	0.1151	0.5421	2.2254	1.1843

105 The saturation state of the sampled fluids reveals that all waters are under saturated with
106 respect to K-feldspar, anorthite (SI from -5.86 to -1.67) albite (SI from -3.08 to -0.56), biotite (SI
107 from -2.15 to -0.98) and are close to the saturation with respect to kaolinite (SI from 0.3 to 4.0)
108 and quartz (SI from 0.31 to 1.20) as well calcite (SI from -0.59 to 0.67). This indicates that the
109 main source of K^+ , Ca^{2+} , Na^+ and Mg^{2+} can be attributed to the dissolution of K-feldspar,
110 plagioclase, albite and biotite respectively.

111 .

112 2.2. Estimation of the reactive surface area

113 The reactive surface area of the minerals participating to water rock interaction in the
114 Jiangxi Province has been estimated assuming the continuum equilibrium hypothesis
115 (Prigogine, 1955; Aagard and Helgeson 1982) and using the water chemical composition as an
116 input data (Marini et al. 2000; Scislewski and Zuddas, 2010). The rate of mineral dissolution
117 “R”, corresponding to the amount of matter released to the fluid per unit of reaction time, is
118 expressed by the following equation (Marini et al., 2000):

$$119 R_i = S_i \cdot \bar{R}_i \quad (1)$$

120 where R is the “*in-situ*” rate of dissolution expressed in *mole per unit of time* representing the
121 mineral dissolution rate under conditions of the thermal water-rock interaction within Jiangxi
122 Province; \bar{R} is an absolute rate of dissolution expressed in $mole \cdot m^{-2} \cdot sec^{-1}$ usually estimated by
123 laboratory experiments and representing the maximum dissolution rate per unit of mineral area;
124 S is the reactive surface area expressed in m^2 . Every member of the Eqn. 1 can be evaluated for
125 each i^{th} mineral phase.

126 Taking into account that water interacts with a multi-mineral system, the overall process
127 can be described by a series of mass balance equations for each of the relevant mineral phases in
128 relation to the reaction rate. Consequently, the dissolution reaction of every main mineral can be
129 associated to the concentration of one of the major cations (Na^+ , K^+ , Ca^{2+} , Mg^{2+}) (Chilakapati,

130 1995; Steefel and MacQuarrie, 1996). Due to difficulties in evaluation the real time of the
 131 reaction, the mass balance equations for every mineral can be solved in a reaction progress mode
 132 (i.e., no time scale provision is needed) by introducing the perturbation progress mode φ
 133 (Prigogine, 1955; Suarez and Wood, 1996; Marini et al., 2000; Scislewski and Zuddas, 2010).
 134 Because thermal waters of Jiangxi Province are of meteoric origin (Chen, 2008; Sun et al., 2016;
 135 Shvartsev et al., 2018), the difference in the water chemical composition can be viewed by an
 136 inflow of deep CO₂ (Chen, 2008; Sun et al., 2014). The perturbation of a system generated by
 137 CO₂ deep inflow can be represented from a starting point 0 to ending point 1. In this case, the
 138 operating variables become a specific function of the advancement of the perturbation φ resolved
 139 in a time-independent space. Considering temperature, pressure, volume and perturbation
 140 progress φ of each specific reaction as an independent variable, the system can be easily solved
 141 by Eqn. 2 (Prigogine, 1955; Sciuto and Ottonello, 1995a, b):

$$142 \quad n_{j,end} - n_{j,start} = \int_{\varphi=0}^{\varphi=1} \left(\sum_i \frac{\partial n_{i,j}}{\partial \varphi_j} \right) d\varphi \quad (2)$$

143 where $n_{j,i}$ stands for the molality of the j^{th} aqueous solute in the i^{th} reaction, φ represents the
 144 perturbation progress, in the considered CO₂ perturbation. Therefore, φ_j can be defined as the
 145 individual perturbation progress related to the j^{th} sampled hot spring. The perturbation progress
 146 can be estimated using the evolution of the normalized progressive major cation concentration
 147 observed in the field by (3) and calculated for each sample of the thermal waters:

$$148 \quad \varphi = n_{Na^+} + n_{Ca^{2+}} + n_{Mg^{2+}} + n_{K^+} \quad (3)$$

149 In result, the lower values of φ indicate weak CO₂ perturbation and the higher values
 150 refer to high perturbed waters. As previous mentioned, to normalize the system and quantify the
 151 perturbation process, all samples were represented from the starting point 0 to ending point 1 and
 152 each individual value of φ_j was divided by a higher or maximum value of φ ($0 \leq \varphi \leq 1$). If φ_j is
 153 close or equal to 0, the system is not perturbed by CO₂, if φ_i is closed or equal to 1 the system is
 154 high perturbed. The variation in concentration within the reaction progress mode becomes
 155 expressed as:

$$156 \quad \frac{dn}{d\varphi} = v \cdot R_\varphi \quad (4)$$

157 where R_φ can be defined as (5):

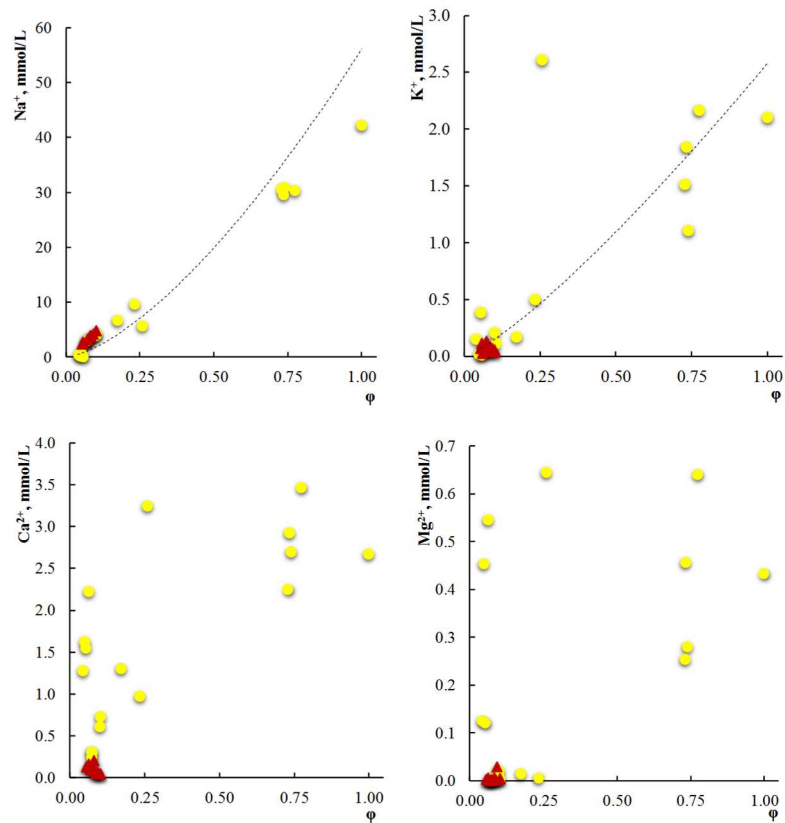
$$158 \quad R_{\varphi_{i,j}} = S_i \cdot \overline{R}_i \left(\frac{dt}{d\varphi} \right) \quad (5)$$

159 $R_{\varphi_{i,j}}$ is the *in-situ* dissolution rate, S_i is the reactive surface area of the i^{th} minerals, \overline{R}_i is a kinetic
 160 function of the reaction affinity and dissolution constants depending on pH, temperature and
 161 chemical composition.

162 The variation in molar concentration of major cations within the perturbation progress
 163 shows that the thermal waters with high $p\text{CO}_2$ (the first group) are the most perturbed while the
 164 thermal waters with low $p\text{CO}_2$ (the second group) are less perturbed (Fig. 4). Additionally, the
 165 most perturbed group is characterized by higher concentrations of cations than the less perturbed
 166 group, as concentrations of Ca^{2+} , Mg^{2+} , K^+ and Na^+ generally increase with CO_2 perturbation
 167 (Fig. 4).

168 According to Eqn. 5, dissolution rates both *in-situ* and laboratory as well reactive surface
 169 area S_i can be calculated independently as a function of the perturbation advancement φ . It
 170 should be noticed that S_i is expressed in square meters per kilogram of water (m^2/kg_w) in contact
 171 with the given mineral surface.

172



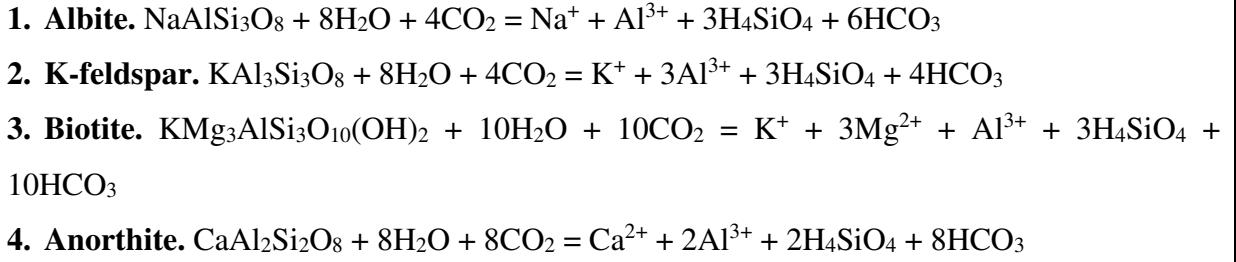
173

174 **Fig. 4** Evolution of molar concentrations of cations as a function of perturbation process
 175 φ .

176 During the overall process, the main dissolved minerals are K-feldspar, biotite and
 177 plagioclases, consequently, the *in-situ* dissolution rate for the individual rock-forming minerals
 178 ($R_{\varphi_{i,j}}$) can be estimated for every sampling spring as the partial derivative of molar concentration
 179 of each cation as a function of the perturbation progress φ (Marini et al., 2000; Scislawski and
 180 Zuddas, 2010).

181 The main chemical reactions controlling the composition of thermal waters are presented
 182 below (Tab. 2). The rate of every reaction can be expressed by the following Eqns:

183 **Table 2.** Chemical reaction controlling the thermal waters composition in Jiangxi Province.



184
$$\frac{d(\text{Na}^+)}{d\varphi} = R_{\text{Albite}} \quad (6)$$

185
$$\frac{d(\text{K}^+)}{d\varphi} = R_{\text{K-feldspar}} \quad (7)$$

186
$$\frac{d(\text{Mg}^{2+})}{d\varphi} = 3R_{\text{Biotite}} \quad (8)$$

187
$$\frac{d(\text{Ca}^{2+})}{d\varphi} = R_{\text{Anorthite}} \quad (9)$$

188 Taking into account that the K-feldspar is the most abundant rock-forming mineral (30-
 189 35%) and biotite is minor (8-10%) (Wang et al., 2012; Tao et al., 2018), we attribute the major
 190 K^+ to the K-feldspar dissolution and the the contribution of biotite dissolution to the K^+ budget is
 191 low. This work attempt to estimate variations of more than one order of magnitude in RSA,
 192 therefore, biotite as a source of K^+ is neglected.

193 The absolute rate of dissolution \bar{R}_i is a function of the reaction affinity according to
 194 Eqn. 10 (Aagard and Helgeson, 1982):

195
$$\bar{R} = k[1 - \exp\left(\frac{A}{RT}\right)] \quad (10)$$

196 where k is the constant dissolution rate, R is the gas constant, T the absolute temperature, and A
 197 is the thermodynamic affinity described by Eqn. 11:

198
$$A = -RT \ln \frac{Q}{K} \quad (11)$$

199 where Q is the ion activity product, K is the mineral solubility constant.

200 The dissolution rate kinetic constant k is conveniently expressed as a semi-logarithmic
 201 function of the system pH by the following Eqn. 12 (Helgeson, 1984; Alekseyev, 1997; Marini et
 202 al. 2000):

203
$$\log k = \log k_0 + b_i(\text{pH} - \text{pH}_0) \quad (12)$$

204 where $\log k_0$ is the value of $\log k$ at $\text{pH} = \text{pH}_0$ and b_i is the slope of the linear function in the $\log k$
 205 vs pH plot. The values of $\log k_0$, b_i and pH_0 were taken from (Marini et al., 2000).

206 The function $(dt/d\varphi)$ and, consequently, the evolution of φ as a function of time cannot be
 207 determined properly because of difficulties in quantification the actual time (Prigogine, 1955). If
 208 we consider the water-rock system and its evolution as irreversible (Shvartsev, 2015), the
 209 derivative ratio $dt/d\varphi$ is a strictly increasing function. Taking into account that $R_{\varphi_{i,j}}$ and S_i cannot

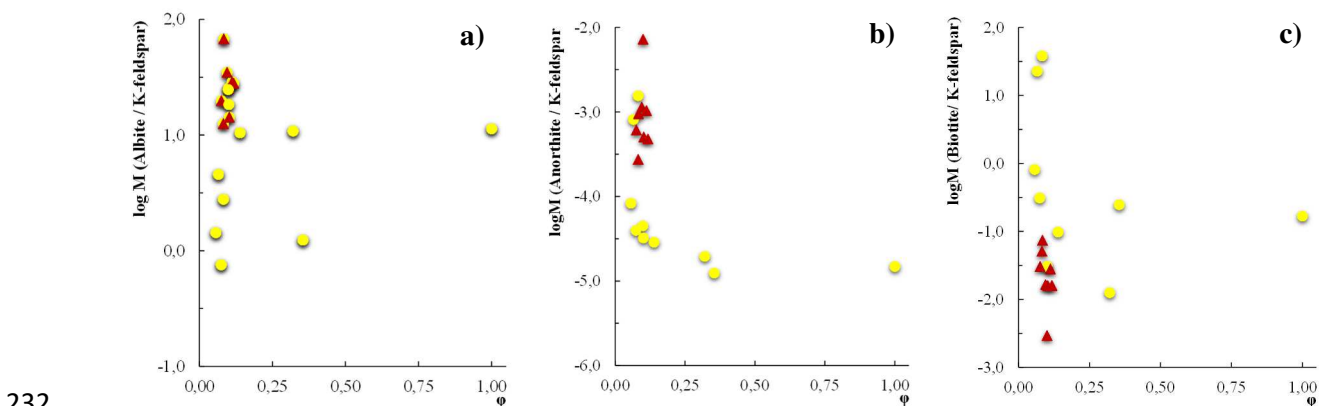
210 be determined as absolute values, the reactive surface area of dissolved minerals has been
 211 quantified as a ratio between different minerals participating in the water-mineral interaction.

212 The variation of reactive surface area of dissolved minerals has been thus estimated as a
 213 ratio (M) between a given mineral and the most abundant mineral in the water-bearing rock
 214 using the following relation expressed by Eqn. 13.

$$215 \quad M = \frac{S_x(dt/d\varphi)}{S_y(dt/d\varphi)} \quad (13)$$

216 where S_x is reactive surface area of rock-forming mineral, S_y is reactive surface area of the most
 217 abundant rock-forming mineral. Therefore, the $(dt/d\varphi)$ can be simplified and the M can be
 218 determined.

219 Petrographic studies (Wang et al., 2012; Tao et al., 2018) indicate that the most abundant
 220 mineral in the water-bearing granite in the Jiangxi Province is a K-feldspar. Therefore, the
 221 reactive surface area of every dissolving mineral (albite, anorthite and biotite) was normalized to
 222 the reactive surface of K-feldspar. The results of RSA ratios for a given mineral obtained in our
 223 study are presented in Tab. 4 and plotted as a function of the perturbation process (φ) in Fig. 5.
 224 We found that the RSA changes by 2-4 orders of magnitude during the perturbation process
 225 indicating that this kinetic parameter cannot be considered as constant during water-rock
 226 interaction processes as currently assumed in transport reaction modelling. The major variation
 227 of all considered reactive surface areas ratios obtained at the weak perturbed state, i. e. φ lower
 228 than 0.25. The reactive surface area ratio of albite/K-feldspar vary within 2 orders of magnitudes
 229 while the reactive surface area of anorthite / K-feldspar ratio changes by 3 orders of magnitude
 230 and the reactive surface area of biotite/ K-feldspar changes within 4 orders of magnitude (Fig.
 231 5c).



232
 233 **Fig. 5.** Evolution of the reactive surface area ratio a) Albite/K-feldspar b) Anorthite/K-feldspar
 234 c) Biotite/K-feldspar as a function of the perturbation process

235 **Table 3.** Results of reactive surface area calculations. The “in-situ” rate of dissolution R expressed in *mole per unit of time*, \bar{R} is an absolute rate of
 236 dissolution expressed in *mole·m⁻²·sec⁻¹*, and S is the reactive surface area.

Spring		<i>Albite</i>			<i>K-feldspar</i>			<i>Anorthite</i>			<i>Biotite</i>			Albite / K-feldspar	Anorthite / K-feldspar	Biotite / K- feldspar	Φ
		log \bar{R}	logR	logS(dt/dφ)	log \bar{R}	logR	logS(dt/dφ)	log \bar{R}	logR	logS(dt/dφ)	log \bar{R}	logR	logS(dt/dφ)				
First group	15-5-1	-16.30	-1.51	14.79	-11.55	-2.50	9.05	-16.55	-4.68	11.87	-17.69	-3.16	13.39	1.39	-4.35	-1.52	0.10
	15-5	-16.29	-1.51	14.78	-11.54	-2.52	9.02	-16.54	-4.54	12.00	-17.68	-3.03	13.51	1.26	-4.49	-1.51	0.10
	15-6	-16.49	-1.55	14.95	-11.74	-2.36	9.39	-16.74	-3.82	12.92	-17.95	-2.82	13.93	1.02	-4.54	-1.01	0.14
	15-4	-16.52	-1.51	15.00	-11.77	-2.65	9.12	-16.77	-3.59	13.17	-17.94	-2.82	13.95	1.06	-4.83	-0.78	1.00
	15-2-1	-16.48	-2.16	14.32	-11.73	-1.64	10.08	-16.73	-2.65	14.07	-17.95	-2.56	14.16	0.16	-4.08	-0.09	0.06
	17-4	-16.33	-2.61	13.73	-11.58	-1.60	9.98	-16.58	-2.16	14.43	-17.85	-3.52	13.07	0.66	-3.09	1.36	0.07
	17-5	-16.35	-3.07	13.28	-11.60	-1.57	10.03	-16.60	-2.18	14.42	-17.85	-3.76	12.83	0.44	-2.81	1.58	0.08
	15-2-2	-16.26	-2.15	14.10	-11.51	-1.68	9.82	-16.51	-2.79	13.72	-17.69	-2.28	14.23	-0.12	-4.40	-0.51	0.07
	15-3	-16.22	-1.52	14.70	-11.47	-2.52	8.95	-16.47	-4.71	11.76	-17.64	-2.81	13.66	1.03	-4.71	-1.90	0.32
	15-1	-16.66	-1.79	14.87	-11.91	-2.04	9.87	-16.91	-2.74	14.17	-18.13	-2.13	14.78	0.09	-4.91	-0.61	0.35
Second group	17-2	-15.84	-1.49	14.35	-11.09	-2.72	8.36	-16.09	-4.70	11.39	-17.35	-3.57	12.52	1.83	-4.15	-1.13	0.08
	17-8	-15.86	-1.49	14.37	-11.11	-2.82	8.29	-16.11	-5.68	10.43	-17.28	-3.15	12.96	1.41	-4.67	-2.53	0.10
	15-7	-15.94	-1.48	14.46	-11.19	-3.00	8.19	-16.19	-5.06	11.13	-17.41	-3.27	12.92	1.54	-4.73	-1.78	0.09
	15-9	-16.00	-1.49	14.51	-11.25	-2.99	8.26	-16.25	-4.69	11.56	-17.37	-2.90	13.35	1.15	-5.09	-1.80	0.10
	17-7	-15.85	-1.50	14.35	-11.10	-2.77	8.32	-16.10	-4.56	11.54	-17.27	-3.04	13.05	1.30	-4.73	-1.52	0.08
	15-10	-15.78	-1.48	14.30	-11.03	-3.29	7.73	-16.03	-4.97	11.05	-17.24	-3.18	12.85	1.45	-5.12	-1.80	0.12
	17-6	-15.93	-1.49	14.44	-11.18	-2.74	8.44	-16.18	-4.76	11.43	-17.37	-3.20	12.98	1.46	-4.54	-1.55	0.11
	15-8	-16.00	-1.51	14.49	-11.25	-2.71	8.54	-16.25	-4.15	12.10	-17.37	-2.86	13.39	1.10	-4.86	-1.29	0.08

3. Discussion and Conclusions

The CO₂ perturbation appears to be the most important factor influencing the composition of the fluids in the Jiangxi Province (Shvartsev and Wang, 2006; Shvartsev et al., 2018). Rising of CO₂ perturbs the water-rock equilibria by the decreasing of fluid pH, enhances mineral dissolution producing an increasing on major cations (Ca²⁺, Mg²⁺, Na⁺, and K⁺) and alkalinity as illustrated in Fig. 6. This process has been quantified in our study and is responsible for modulating the release of deep CO₂ to the atmosphere in this area.

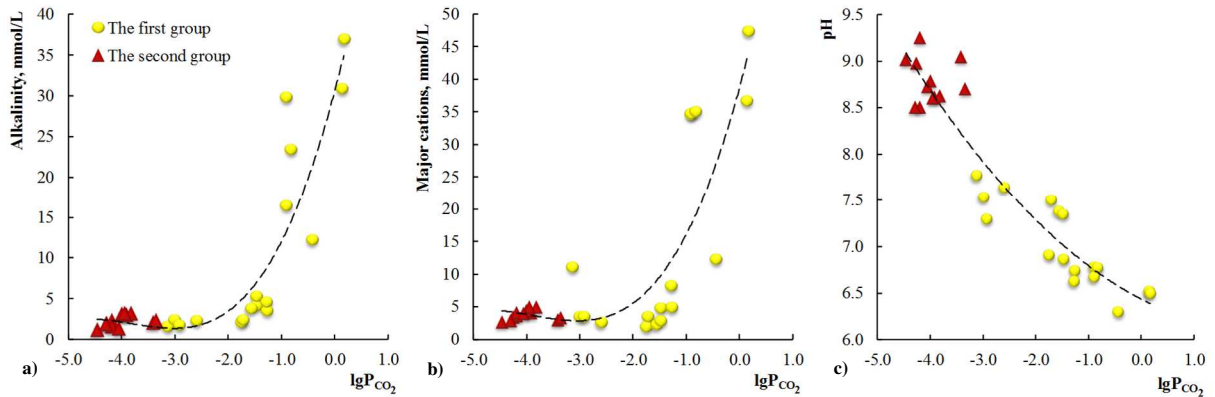


Fig. 6. Dependence of alkalinity (a), major cations content (b) and pH (c) on the partial pressure of CO₂ in the thermal waters of Jiangxi Province

The evaluated RSA ratios show that the biotite/ K-feldspar contribution is wider compared to that of other mineral ratios (Fig. 5c) indicating the significant contribution of biotite dissolution in complex process of CO₂ releasing. The high contribution of biotite to CO₂ neutralization was unexpected as biotite is not a major mineral constituent in granites. Our results showing the significant contribution to biotite during granite-water interaction are in agreement with earlier estimations in the Cornish hydrothermal granite-interaction (Edmunds et al., 1985) and in French areas (Zuddas and Rillards, 2013). Moreover, RSA of the main rock-forming minerals is lower in alkaline thermal waters (pH>8) where possible secondary minerals may overlay primary ones reducing the surface area of interaction (Fig.7).

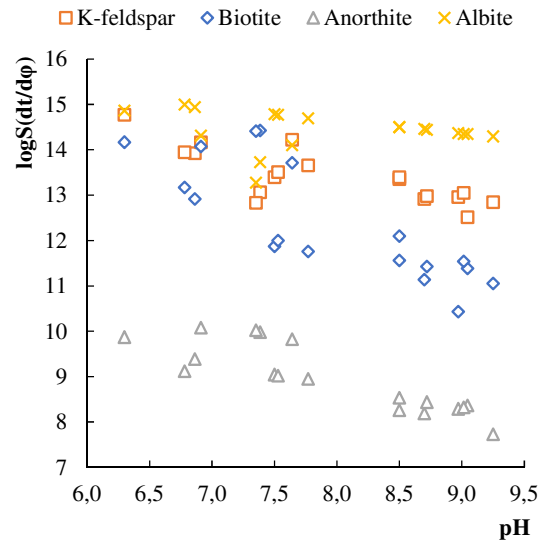


Fig. 7. The correlation between the reactive surface area changes and pH values of the thermal waters

Taking into account the geological and tectonic conditions of different thermal waters occurrence in Jiangxi Province, their saturation state to different minerals and calculated RSA ratios, we propose a conceptual model explaining the thermal water formation in the studied area (Fig. 8). The geothermal field of Jiangxi Province can be viewed as a result of water-granite interaction, perturbed by CO₂ influxes. At the emergence, thermal waters are characterized by different P_{CO₂} and chemical composition, resulting from different reactivity to the CO₂ perturbation. Taking into account the water chemical composition and pCO₂ dependency (Fig. 3), the studied waters have been viewed by a continuous water-rock interaction perturbed by CO₂ limited by two end-members. These waters are of meteoric origin (Chen, 2008; Shvartsev et al., 2018) reaching an estimated deep temperatures varying between 62° and 153 °C for the first group and between 85 and 147 °C for the second group as estimated by the silica geothermometer (Fournier, 1977). These values correspond to a 25 °C/km geothermal gradient (Wan, 2012) suggesting a water circulation until 2.8-5.3 km depth for the group of low CO₂ and to 1.8-5.6 km for the group of high CO₂ (Li and Li, 2010).

In case of first-group, CO₂ of deep origin (Chen, 2008) enters the thermal aquifer, perturbs the system (Shvartsev and Wang, 2006; Shvartsev et al., 2018) leading to mineral dissolution and influencing strongly the reactive surface areas of biotite. In case of second-group, CO₂ is consumed by mineral dissolution and waters reach higher pH with possible neof ormation of clay minerals, e.g. kaolinite that is in agreement with the results of thermodynamic equilibrium modeling (Sun et al, 2016; Sun et al., 2017; Zippa, 2017; Shvartsev et al, 2018).

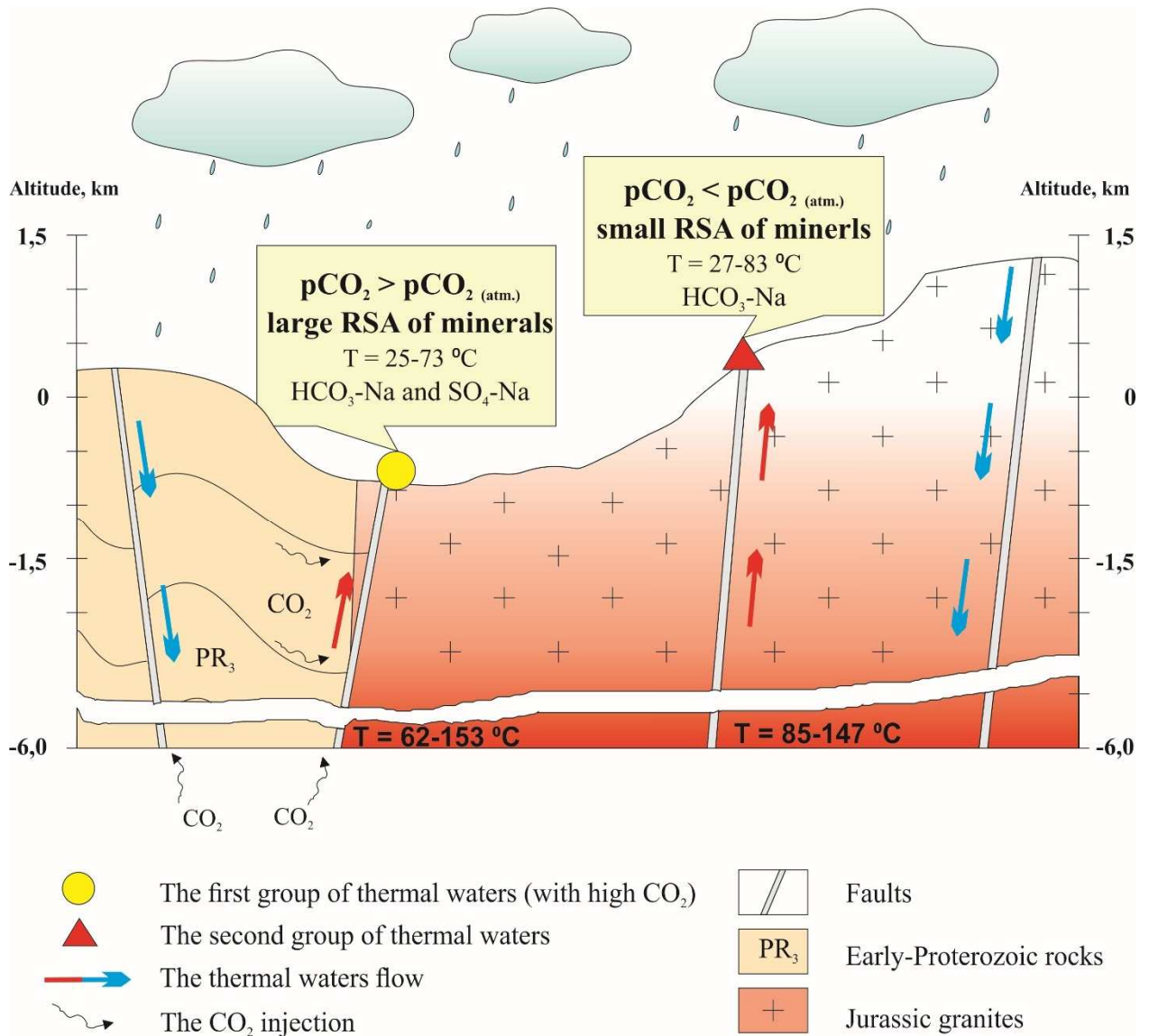


Fig. 8. Conceptual model of the thermal water formation in Jiangxi Province

To summarize, meteoric water enters the rock, heat up, dissolve primary minerals and interact with the CO₂ of deep origin leading to the thermal water formation. CO₂-inflow perturbs the thermal water composition resulting in two groups of thermal waters. The first group is characterized by higher pCO₂, low pH, high reactive surface area of dissolving minerals. The second group is characterized by low pCO₂, high pH and lower reactive surface area compared to the first group.

Finally, the results of reactive surface area of the mineral estimations show the significant contribution of the biotite dissolution in CO₂-neutralizing processes that may play a key role in the formation of the alkaline thermal water (second group) in Jiangxi Province.

Acknowledgements

The study was partially financially supported by a grant from Russian Science Foundation [grant number 17-17-01158] and from the President of Russian Federation Scholarship Program. Work is supported by State program RF «Science». Project FSWW-0022-2020. We also thank an anonymous and Prof. M. Kersten for their important contribution that significantly improved the quality and the clarity of the manuscript.

References

- Aagaard, P., Helgeson, H.C., 1982. Thermodynamic and kinetic constraints on reaction rates among minerals and aqueous solutions. I. Theoretical considerations. *Am. J. Sci.* 282, 237-285.
- Alekseyev, V. A., Medvedeva, L. S., Prisyagina, N. I., Meshalkin, S. S., Balabin, A., 1997. Change in the dissolution rates of alkali feldspars as a result of secondary mineral precipitation and approach to equilibrium. *Geochim. et Cosmochim. Acta.* 59, 19-31.
- Bolourinejad. P., Shoeibi Omrani. P., Herber. R., 2014. Effect of reactive surface area of minerals on mineralization and carbon dioxide trapping in a depleted gas reservoir. *Int. J. Greenhouse Gas Control* 21, 11-22.
- Bethke, C.M., Farrell, B., Yeakel, S., 2018. *The Geochemist's Workbench, Version 12.0: GWB Essentials Guide. Aqueous Solutions. LLC, Champaign, Illinois, US.*
- Chen, G., 2008. The isotopic and chemical characteristics of geothermal fluids from the Western fjords, Iceland and two selected hot spring areas in Jiangxi Province, SE-China. *Geothermal training programme. Reports*, 13, 32 p.
- Chilakapati, A., 1995. RAFT: A simulator for reactive flow and transport of groundwater contaminants. PNL-10636, Pacific Northwest Laboratory Report.
- Edmunds, W. M., Kay, RLF, McCartney, R.A., 1985. Origin of saline groundwaters in the Carnmenellis Granite (Cornwall. England): Natural processes and reaction during Hot Dry Rock reservoir circulation. *Chem. Geol.* 49, 287-301.
- Fournier, R.O., 1977. Chemical geothermometers and mixing models for geothermal systems. *Geothermics.* 5, 41-50.
- Garrels, R.M., 1960. *Mineral Equilibria at low temperature and pressure.* N.Y.: Harper and Row, New York, 306 p.
- Geological memoirs, 1984. *An Outline of the Regional Geology of Jiangxi Province. Ser. 1. N. 2. Regional Geology of Jiangxi Province.* Beijing. Geological publishing house (People's Republic of China, Ministry of Geology and Mineral Resources. Jiangxi Bureau of Geology and Mineral Resources), China p. 922.

- Gouze, P., Luquot, L., 2011. X-ray microtomography characterization of porosity, permeability and reactive surface changes during dissolution. *J. Contam. Hydrol.* 120-121, 45-55.
- Helgeson, H. C., Murphy, W. M., Aagaard, P., 1984. Thermodynamic and kinetic constraints on reaction rates among minerals and aqueous solutions. II. Rate constants, effective surface area, and the hydrolysis of feldspar. *Geochim. Cosmochim. Acta.* 48, 2405-2432.
- Li, G., Li, F., 2010. *The Circulation Law, Sustainable Development and Utilization of Geothermal Water in Guanzhong Basin.* Science press, Beijing, p. 100.
- Li, X., 1979. The relationship between distribution of thermal waters and uranium mineralization in Jiangxi. *J. of East China Geol. Inst.* 21-29.
- Marini, L., Ottonello, G., Canepa, M., Cipolli, F., 2000. Water-rock interaction in the Bisagno valley (Genoa, Italy): application of an inverse approach to model spring water chemistry. *Geochim. Cosmochim. Acta.* 64, 2617-2635.
- Prigogine I., 1955. *Introduction to Thermodynamics of Irreversible Processes.* 2nd edition, Interscience Publishers, New York, 147 p.
- Scislawski, A. Zuddas, P., 2010. Estimation of reactive mineral surface area during water-rock interaction using fluid chemical data. *Geochim. Cosmochim. Acta.* 74, 6996-7007.
- Sciuto, P. F., Ottonello, G., 1995a. Water-rock interaction on Zabargad Island (Red Sea), a case study: I. Application of the concept of local equilibrium. *Geochim. Cosmochim. Acta.* 59, 2187-2206.
- Sciuto, P. F., Ottonello, G., 1995b. Water-rock interaction on Zabargad Island (Red Sea), a case study: II. from local equilibrium to irreversible exchanges. *Geochim. Cosmochim. Acta.* 59, 2207-2214.
- Shvartsev, S.L., 2015. The basic contradiction that predetermined the mechanisms and vector of global evolution. *Her. Rus. Acad. Sci.* 85 (4), 342-351.
- Shvartsev, S.L., Sun, Z., Borzenko, S.V., Gao, B., Tokarenko, O.G., Zippa, E.V., 2018. Geochemistry of the thermal waters in Jiangxi Province, China. *Appl. Geoch.* 96, 113-130.
- Shvartsev, S.L., Wang, Y.X., 2006. Geochemistry of sodic waters in the Datong intermountain basin, Shanxi Province, northwestern China. *Geochem. Int.* 44 (10), 1015-1026.
- Steeffel, C. I., MacQuarrie, K. T. B., 1996. Approaches to modeling of reactive transport in porous media. In *Reviews in Mineralogy* (eds. P. C. Lichtner, C. I. Steefel, and E. H. Oelkers), Mineralogical Society of America, Washington D.C. 34, 83-129.
- Suarez, D.L., Woods, J.D., 1996. Short- and long-term weathering rates of a feldspar fraction isolated from an arid zone soil. *Chem. Geol.* 132, 143-150.

- Sun, Z., Gao, B., Zhang, Z. 2014 Isotopic evidence for origin of geothermal gases from hot springs in southern Jiangxi Province, SE-China. *Chin. Jour. of Geol.* 49 (3), 791-798 [in Chinese].
- Sun, Zh, Gao, B., Shvartsev, S., Tokarenko, O., Zippa, E., 2017. The thermal water geochemistry in Jiangxi province (SE-China). *Procedia Earth and Planetary Science* 17, 940–943.
- Sun, Zh, Li, X., 2001. Studies of geothermal waters in Jiangxi Province using isotope techniques. *Science in China (Series E)* 44, 144-150.
- Sun, Zh., Shvartsev, S.L., Tokarenko, O.G., Zippa, E.V., Gao, B., 2016. Geochemical peculiarities of nitric thermal waters in Jiangxi province (SE-China). *IOP conference series: earth and environmental science: all-Russian scientific conference with international participation on contemporary issues of hydrogeology. Engineering Geology and Hydrogeoecology in Eurasia 23–27 November 2015, Tomsk, Russia.* 33(1), 6.
- Tao, J., Li, W., Wyman, D. A., Wang, A., Xu, Zh., 2018. Petrogenesis of Triassic granite from the Jintan pluton in Central Jiangxi Province, South China: implication for uranium enrichment. *Lithos.* 320–321, 62-74.
- Wan, T., 2012. *The Tectonics of China. Data, Maps and Evolution.* Springer-Verlag Berlin Heidelberg, 506 p.
- Wang, G.-G., Ni, P., Zhao, K.-D., Wang, X.-L., Liu, J.-Q., Jiang, S.-Y., Chen, H., 2012. Petrogenesis of the Middle Jurassic Yinshan volcanic-intrusive complex, SE China: Implications for tectonic evolution and Cu-Au mineralization. *Lithos.* 150, 135-154.
- Zhou, W., 1996. *Studies of Geothermal Background and Isotopic Geochemistry of Thermal Water in Jiangxi Province.* China Nuclear Science and Technology report, 29 p.
- Zippa, E.V., 2017. Equilibrium-nonequilibrium state of the system of nitrogen rich thermal waters and rocks in Jiangxi province (SE China). *XXI international scientific Symposium in honor of Academician M.A. Usov “problems of geology and Subsurface development”.* Tomsk, TPU 2, 998–1000.
- Zuddas, P., Rillard, J., 2013. Estimating the Reactive Surface Area of Minerals in Natural Hydrothermal Fields: Preliminary Results. *Procedia Earth and Planetary Science*, 7, 953-957.